ADVANCED MATERIALS
www.advmat.de

Microneedle-Mediated Delivery of Immunomodulators Restores Immune Privilege in Hair Follicles and Reverses Immune-Mediated Alopecia

Nour Younis, Núria Puigmal, Abdallah El Kurdi, Andrew Badaoui, Dongliang Zhang, Claudia Morales-Garay, Anis Saad, Diane Cruz, Nadim Al Rahy, Andrea Daccache, Triana Huerta, Christa Deban, Ahmad Halawi, John Choi, Pere Dosta, Christine Guo Lian, Natalie Artzi, and Jamil R. Azzi**

Disorders in the regulatory arm of the adaptive immune system result in autoimmune-mediated diseases. While systemic immunosuppression is the prevailing approach to manage them, it fails to achieve long-lasting remission due to concomitant suppression of the regulatory arm and carries the risk of heightened susceptibility to infections and malignancies. Alopecia areata is a condition characterized by localized hair loss due to autoimmunity. The accessibility of the skin allows local rather than systemic intervention to avoid broad immunosuppression. It is hypothesized that the expansion of endogenous regulatory T cells (T_{regs}) at the site of antigen encounter can restore the immune balance and generate a long-lasting tolerogenic response. A hydrogel microneedle (MN) patch is therefore utilized for delivery of CCL22, a T_{reg}-chemoattractant, and IL-2, a T_{reg} survival factor to amplify them. In an immune-mediated murine model of alopecia, local bolstering of T_{reg} numbers is shown, leading to sustained hair regrowth and attenuation of inflammatory pathways. In a humanized skin transplant mouse model, expansion of T_{regs} within human skin is confirmed without engendering peripheral immunosuppression. The patch offers high-loading capacity and shelf-life stability for prospective clinical translation. By harmonizing immune responses locally, the aim is to reshape the landscape of autoimmune skin disease management.

1. Introduction

Impairment of self-tolerance in the skin is the driving factor of most cutaneous autoimmune diseases including vitiligo, alopecia areata (AA), pemphigoid and pemphigus, psoriasis, and systemic sclerosis.[1] Regulatory T cells (T_{regs}) are a subset of T cells responsible for maintaining immune homeostasis and immune tolerance to both self and non-self-antigens.[2,3] Changes in their number and/or function are key contributors to the pathogenesis of these skin diseases.[4] AA is a T-cell mediated autoimmune disease that provokes hair loss in hair-bearing areas with a relapsing/remitting chronic course.[5,6] It affects all sex and ethnic subgroups and inflicts devastating social and psychological implications on the affected population (around 3% of the general population) since there is no cure for it.[7–9] AA manifests in the hair follicles (HFs) during the anagen phase of hair growth and emanates from the disruption of the HF immune privilege, in which the bulge region downward to the

N. Younis, A. Badaoui, D. Zhang, A. Saad, N. A. Rahy, A. Daccache, C. Deban, A. Halawi, J. Choi, J. R. Azzi
Brigham and Woman's Hospital, Department of Medicine, Renal Division
Harvard Medical School
Boston, MA 02115, USA
E-mail: jazzi@bwh.harvard.edu

N. Puigmal, C. Morales-Garay, D. Cruz, T. Huerta, P. Dosta, N. Artzi
Brigham and Woman's Hospital, Department of Medicine, Division of Engineering in Medicine
Harvard Medical School
Boston, MA 02115, USA
E-mail: nartzi@bwh.harvard.edu

The ORCID identification number(s) for the author(s) of this article can be found under https://doi.org/10.1002/adma.202312088

DOI: 10.1002/adma.202312088

N. Puigmal, P. Dosta, N. Artzi
Institute for Medical Engineering and Science
Massachusetts Institute of Technology
Cambridge, MA 02138, USA

N. Puigmal, P. Dosta, N. Artzi
Wyss Institute for Biologically Inspired Engineering
Harvard University
Boston, MA 02215, USA

A. E. Kurdi
Department of Biochemistry and Molecular Genetics, Faculty of Medicine
American University of Beirut
Beirut 11-0236, Lebanon

C. Guo Lian
Department of Pathology
Brigham and Women's Hospital
Boston, MA 02115, USA

hair bulb loses protection against undesired immune responses such as the disruption of T_{reg} homeostasis.[10] Many studies have noted a deficiency of T_{regs} in AA lesions[11] and more recently, the crucial role of T_{regs} in disease progression was demonstrated as impairment of skin-specific T_{regs} sufficed to trigger alopecia and HF inflammation.[12] Along with T_{reg} disruption, HF-associated peptides lead to the chemoattraction and stimulation of autoreactive T cells including T-helper 1 lymphocytes, cytotoxic CD8 T cells, and natural killer (NK) cells that infiltrate into the HF that disrupt the immune privilege.

The first line-of-defense for managing AA involves off-label use of corticosteroids or prescription of Janus Kinase (JAK) inhibitors, the only FDA-approved therapy for severe AA cases. While JAK inhibition can suppress autoreactive T cells, it also suppresses T_{regs} by inhibiting the phosphorylation and activation of the transcription factor STAT5, which is essential for T_{reg} function.[13,14] potentially disrupting the ability for long-term generation of immune tolerance. This may also explain the high recurrence rates seen after treatment withdrawal (>50%).[15,16] Also their immunosuppressive nature leads lead to heterogenous risks of infection, cardiovascular events, and malignancies, deterring its use for patients with mild-to-moderate symptoms (up to 90% of all AA patients)[9] as the risk outweighs the benefit.[17,18]

We and others have hypothesized that long-lasting remission of immune-mediated diseases will occur only if the treatment can concomitantly control inflammation and restore T_{reg} function and count.[19] Here, we sought to study the extent by which T_{reg}-tropic immunomodulators can suppress cytotoxic T cells while amplifying T_{regs} in the lesion to reinstate HF immune privilege. We therefore used a hydrogel-based microneedle (MN) patch, composed of hyaluronic acid (HA) to deliver CCL22 and IL-2 for T_{reg} recruitment and expansion, respectively. We show that our engineered polymeric microneedle platform supports local delivery of the immunomodulators in the affected skin lesions of an immune-mediated alopecia model and results in remodeling of the local milieu. This results in the restoration of HF immune privilege and therefore hair regrowth, without inducing systemic immunosuppression. We also found that our MNs induce Treg expansion in a humanized skin transplant murine model, confirming the translational potential of our platform into clinical settings.

Furthermore, we and others have demonstrated the diagnostic potential of MNs as means to sample interstitial skin fluid (ISF), a unique biofluid offering insights into disease-specific biomarkers.[20] The HA matrix of our MN platform has been engineered to contain disulfide bonds, enabling us to dissolve the needles following retrieval and isolate cellular biomarkers that can be used to report on the disease state.[21–23] Here, we show that the T cell immune profile in ISF when extracted with the MNs correlates with that in the skin. Our immunoregulatory, rather than immunosuppressive, approach through the use of MNs has the potential to overcome the pitfalls of current AA treatments and other autoimmune skin diseases, while enabling non-invasive monitoring of therapy efficacy via longitudinal ISF sampling.

2. Results

2.1. AA Is Characterized by T_{reg} Deficiency That Can Be Restored via an Immunoregulatory Approach

We hypothesized that T_{reg} expansion in AA lesions will improve the therapeutic outcomes given their crucial role in the pathogenesis of the disease. Hence, we analyzed publicly-available single-cell RNA sequencing data of immune cells in human and murine AA to understand the T_{reg} fingerprint in AA.[24] We found the IL-2/STAT5 signaling pathway to be the most upregulated pathway in AA-infiltrating T_{regs} compared to the rest of the immune cells, in both human and murine AA lesions (**Figure 1**a–d). We, therefore, proposed to harness this pathway using MNs delivering IL-2, which will preferentially promote T_{reg} proliferation, along with CCL22, a potent T_{reg} chemoattractant, to attract and expand T_{regs} locally in the HF milieu and restore self-tolerance in the context of AA (Figure 1e). Our MN patch with a matrix of HA crosslinked to an 8-arm-PEG.[24] and consisting of an array of 121 needle projections sizing 600 µm in length (Figure 1f) was used to evaluate the effect of IL-2 delivery on T_{reg} stability and survival when compared to the standard-of-care for adults with severe AA, the JAK inhibitor baricitinib. Briefly, MNs loaded with either IL-2 or baricitinib were incubated in vitro with T_{regs} purified from the splenocytes of C57BL/6 mice, and the survival (Figure 1g) and stability (Figure 1h) of T_{regs}, reflected by the percentage of $CD4^+CD25^+Foxp3^+$, were measured by flow cytometry at 72 h post-incubation. We found that T_{regs} incubated with empty MNs (negative control) displayed reduced survival and low levels of Foxp3 expression. Instead, IL-2-loaded MNs were capable of inducing superior T_{reg} stability and survival, similar to the levels induced by an equal concentration of soluble IL-2, confirming that the biological activity of the immunomodulators is maintained when loaded into the MNs. Additionally, we tested the effect of baricitinib on T_{regs}, in particular, on their stability and survival by incubating the T_{regs} with baricitinib-loaded MNs or with soluble baricitinib. In both cases, we found that T_{reg} homeostasis was impaired, which was hypothesized to be caused by the inhibitory effect of baricitinib on STAT5—a key mediator of T_{reg} proliferation. Moreover, we confirmed that the detrimental effects of baricitinib on T_{reg} survival and stability could not be salvaged by the addition of soluble IL-2 as the percentage of live and stable T_{regs} was significantly lower (<50%) than those reported when using IL-2-loaded MNs or its soluble homologous (Figure 1g,h). These findings along with the RNA-sequencing analysis prompted us to pursue the delivery of IL-2, along with CCL22, to promote T_{reg} expansion.

We next characterized the MN platform with a focus on clinical translation. Assessment of the mechanical properties of the HA-MNs when loaded with increasing concentrations of IL-2 confirmed that the mechanical strength of the MN patch was not impacted by the drug loading, as tested by compression test (Figure S1a, Supporting Information). We also assessed the biological activity of the immunomodulators loaded in the MNs when stored under different temperatures and over different periods of time (from 1 week to 1 year). We confirmed that when loaded in the MN patch, IL-2 remains stable and

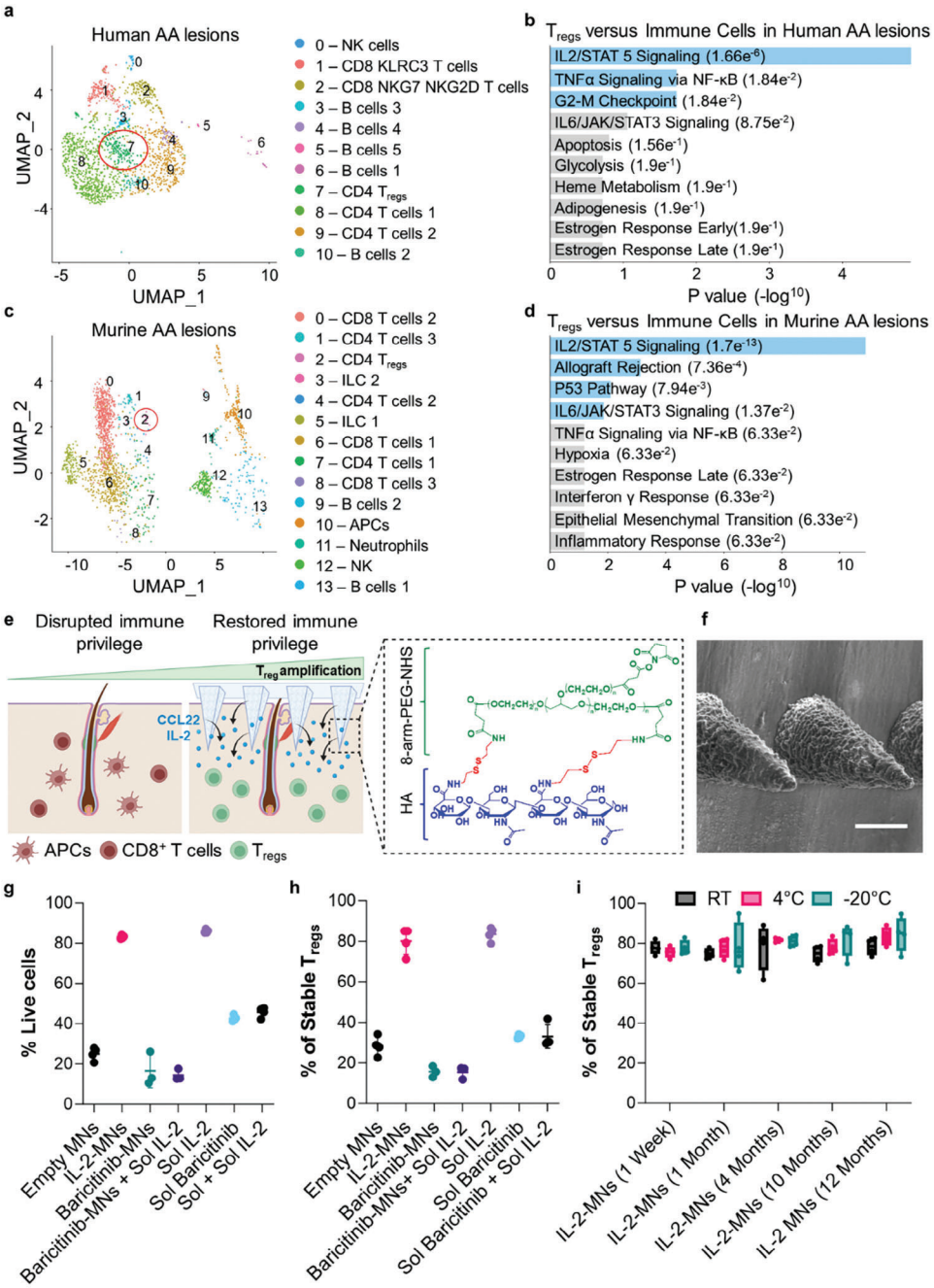

Figure 1. a) UMAP depicting the different clusters of immune cells infiltrating human AA lesions, and b) table highlighting the pathways upregulated in human AA-infiltrating T_{regs} versus all other immune cells (non-T_{regs}). c) UMAP showing the different clusters of immune cells infiltrating murine AA lesions, and d) table showing the pathways upregulated in murine AA-infiltrating T_{regs} versus non-T_{regs}. e) Schematic representation of T_{reg}-amplifying MNs to restore the immune privilege in the HFs. f) Scanning Electron Microscopy (SEM) image depicting HA-derived MNs. Scale bar = 200 µm. Quantification of g) survival and h) stability of T_{regs} isolated from C57BL/6 mice incubated with soluble IL-2, soluble baricitinib, empty MNs, IL-2-loaded MNs, and baricitinib-loaded MNs. i) Functional activity of IL-2 when loaded into the HA-MNs was gauged by comparing T_{reg} stability after incubation with MNs stored at different temperatures (20, 4, −20 °C) for increasing periods of time (1 week up to 1 year). Multiple comparisons among groups were determined using one-way ANOVA. A *p*-value less than 0.0001 was noted between the empty MNs group and all other groups. No statistically significant differences were observed between the different temperatures and/or time points.

therefore retains its biological activity regardless of the storage temperature and time (Figure 1i). When stored at room temperature and shielded from humidity, the performance of 1-week and 1-year-old MNs was comparable (Figure 1i). Moreover, storage temperature did not appear to impact the biological activity of IL-2, since T_{reg} stability was maintained (Figure 1i), confirming the clinical relevance of the platform. We also aimed to study the changes in the protein structure upon elution from the MNs by using Liquid chromatography-mass spectrometry (LC-MS), further confirming that the protein remained intact upon release as no differences in the sequence were observed when compared to soluble IL-2 (Figure S1b, Supporting Information).

2.2. MN-Mediated Delivery of IL-2 and CCL22 Results in Local Expansion of T_{regs} Only in the Immune-Mediated Alopecia Lesions but Not Peripherally

Next, we evaluated the therapeutic potential of our immunomodulatory platform in vivo, in particular, its effect on T_{reg} expansion, using an immune-mediated AA-like phenotype in a murine model as described by others[25] which manifests in patchy hair loss. The therapeutic regimen consisted of serial applications, every other day (ten times), of 1 MN patch into the affected lesion loaded with both CCL22 (100 ng patch^{-1}) and IL-2 (10 ng patch^{-1}) to mediate the recruitment and proliferation of T_{regs}, respectively. The other experimental groups were administered with empty MNs following the same regimen or were left untreated, serving as control groups.

Briefly, we harvested the AA-like skin lesions of all mice at week 3 (right after treatment discontinuation) of the untreated mice, mice administered with empty MNs, and mice administered with IL-2+CCL22-loaded MNs and characterized the immune profile by flow cytometry. A significant reduction in immune infiltration was noted in mice treated with loaded MNs compared to those treated with empty MNs and the untreated group, as reflected by both percentage (4.6% versus 7.335% (p = 0.17) and 9.27% (p = 0.01)) and absolute counts of $CD45^+$ cells infiltrating into the skin lesions (6772 versus 11 698 (p = 0.2) and 14 204 cells (p = 0.04)) (**Figure 2a,b**). Next, the percentage and count of live T_{regs} in the AA-like lesions were used to examine the effect of our platform on T_{reg} recruitment and proliferation. Mice treated with IL-2+CCL22-loaded MNs showed significantly increased percentages of T_{regs} (gated as $CD4^+CD25^+Foxp3^+$) compared to those treated with empty MNs and the group left untreated respectively (5.9%, 1.36% (p = 0.02), and 0.47% (p = 0.007)) and count (312, 139 (p = 0.04), and 68 cells (p = 0.004)) (Figure 2a,b), confirming the ability of our platform to expand T_{regs} in the treated lesions. Additionally, mice treated with IL-2+CCL22-loaded MNs displayed a significant decrease in the count of cytotoxic effector $CD8^+$ T cells and their cytotoxicity as gauged by the expression of pro-inflammatory cytokines such as TNFα and IFNγ (Figure S2, Supporting Information). To examine the systemic immune effect of our platform, we isolated peripheral lymphoid organs including spleen and draining lymph nodes of AA lesions and quantified T_{reg} proliferation. Remarkably, we did not observe significant differences between the T_{reg} percentage in the untreated and the treated groups with loaded MNs at any time point (Figure S3, Supporting Information), confirming that local delivery of IL-2 does not promote peripheral T_{regs} expansion.

2.3. Hallmark Inflammatory Pathways Are Inhibited in AA-Like Lesions Following MN Treatment as Confirmed by Unbiased RNA Sequencing Analysis

We next evaluated the effect of our platform on the immune hallmarks of the disease at the gene level using an unbiased approach, RNA-seq analysis. Briefly, we harvested the AA-like skin lesions from the three different experimental groups (untreated, treated with empty MNs, and treated with IL-2+CCL22 loaded MNs) at week 3 and isolated the genetic material for successive analysis. We first analyzed the inflammatory gene expression signatures of the AA Disease Severity Index (ALADIN index.),[26,27] a 3D quantitative score that can be used to gauge disease severity and response to treatment.[27] The ALADIN signature genes including CD8a, GZMB, ICOS, PRF1, CXCL9, CXCL10, CXCL11, and STAT1 were significantly downregulated in the groups treated with IL-2+CCL22 and empty MNs compared to untreated (Figures 2c and S2, Supporting Information). Next, gene set enrichment analysis was conducted to identify the molecular pathways that are differentially expressed among the different experimental groups. Four key AA inflammatory pathways (IL6-JAK-STAT3 signaling, inflammatory response, IFNγ response, and antigen processing and presentation) were significantly downregulated in the immune-mediated alopecia lesions treated with IL-2+CCL22-loaded MNs (Figure 2e). For instance, IFNγ response was 2.33-fold and 1.79-fold more upregulated in the untreated group, and the group treated with empty MNs, respectively, compared to the group treated with IL-2+CCL22 MNs. These results confirm that the IFNγ signature, essential for AA development and persistence, was significantly suppressed in the group treated with IL-2+CCL22-loaded MNs, highlighting the therapeutic benefit of T_{regs} homing to the affected skin. Additionally, the antigen processing and presentation pathways were downregulated in mice administered with IL2+CCL22-loaded MNs, confirming that our MNs were mitigating crucial inflammatory roles contributing to the pathogenesis of AA. Another imperative inflammatory pathway, the IL-6-JAK-STAT3 signaling pathway, was also downregulated in the lesions treated with IL2+CCL22-loaded-MNs, when compared to untreated and group treated with empty MNs (Figure 2e). These findings align with the abovementioned immune phenotyping data that suggested a significant decrease in infiltrating immune cells in the lesions treated with loaded MNs.

2.4. IL-2+CCL22 MNs Reduce Long-Term Inflammation and Restore HF Structures in AA-Like Lesions

We next gauged the immunomodulatory effect of the platform on week 6 post-treatment initiation by quantitative PCR (RT-PCR) where Foxp3 was used as the differential transcription factor of T_{regs} and IFNγ as a pro-inflammatory biomarker. Foxp3 expression was significantly upregulated in immune-mediated AA

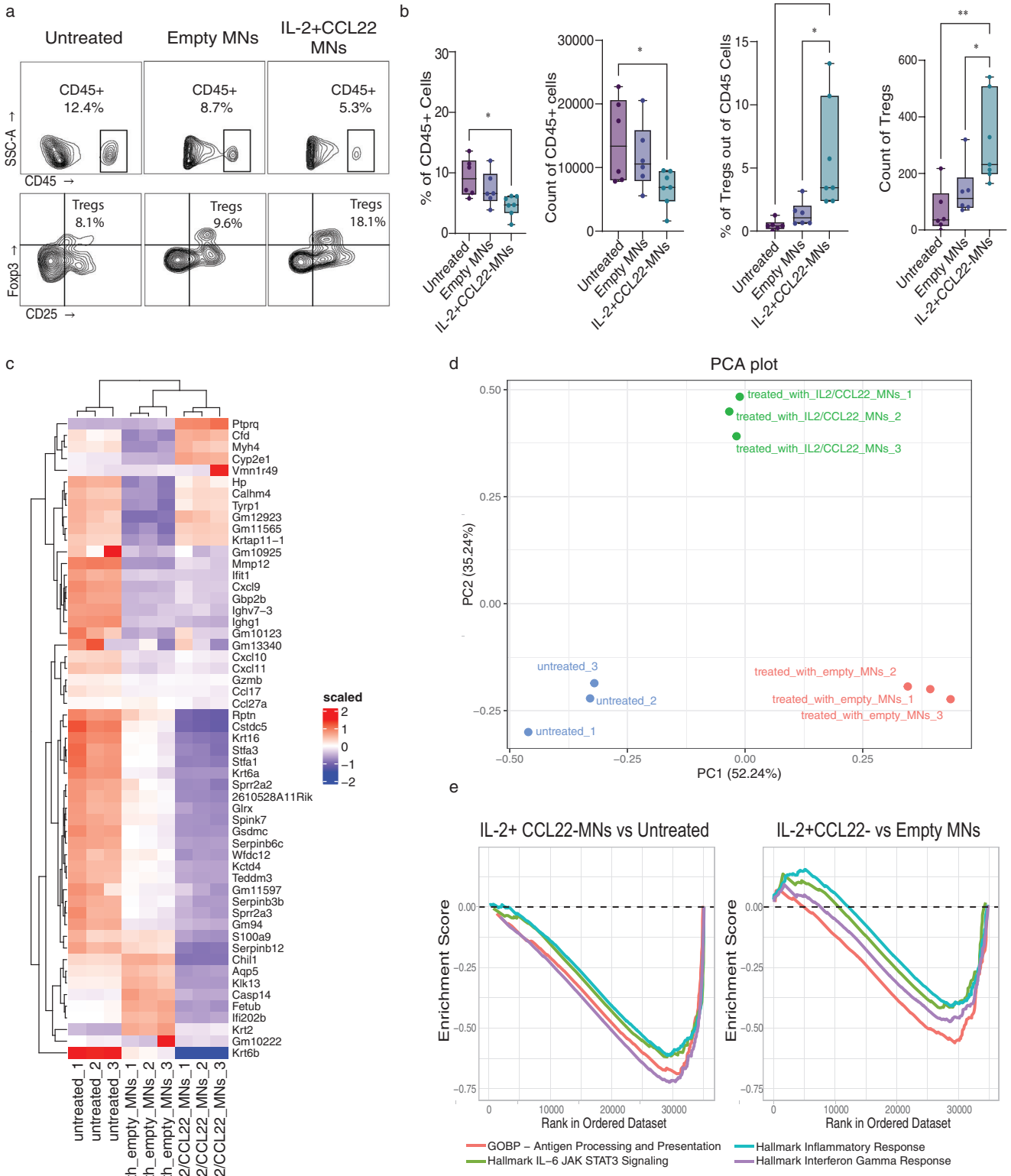

lesions treated with IL-2+CCL22-loaded MNs whereas IFNγ expression was significantly reduced in the lesions treated with IL-2+CCL22-loaded MNs compared to untreated lesions and to those treated with empty MNs (Figure S4a,b, Supporting Information).

To further confirm our findings, we analyzed the changes in the immune signature at the tissue level by histology. Affected skin lesions harvested for mechanistic analysis (6 weeks post-treatment-initiation) were sectioned and stained as described in the Experimental Section. H&E staining confirmed reversal of the histological biomarkers of the disease in those mice treated with IL-2+CCL22-loaded MNs and to a lesser extent, in those administered empty MNs. Specifically, a higher number of healthy HF structures were observed; instead, they appeared to be damaged in untreated mice. Additionally, the epidermis of the affected untreated lesions was significantly thicker than the epidermal layer of IL-2+CCL-2 MNs treated lesions highlighting an attenuation of the chronic inflammation induced by IFNɣ and polyinosinic:polycytidylic acid (poly[I:C]), as suggested by others (Figure S4c, Supporting Information).[25] Moreover, FoxP3 staining revealed a higher T_{reg} infiltrate in the lesions treated with CCL22 and IL-2, whereas fewer T_{regs} were observed in the control groups. Finally, $CD8^+$ T cell infiltrates appeared to be reduced in treated lesions as opposed to the control groups that received empty MNs or were left untreated, where higher presence of lymphocytic infiltrates was observed, and in some instances surrounding the HF shaft in agreement with the literature.[25]

2.5. IL-2+CCL22 MNs Induce More Immune Regulation Than IL-2 Only MNs and Baricitinib-Loaded MNs

Based on our in vitro findings, we next compared the effect of IL-2+CCL22 MNs on the immune signature of the AA-like lesions to the standard-of-care for severe cases, baricitinib. Following the same treatment regimen as before, mice were administered either IL-2+CCL22-loaded MNs, baricitinib-loaded MNs, or IL-2-loaded MNs without CCL22. Flow cytometry analysis revealed a statistically significant reduction in cells that serve as hallmark of the disease, IFNγ^+ cytotoxic $CD8^+$ cells, in all mice treated with MNs compared to the untreated group (8.3%, 1.8% ($p = 0.004$), 1.7% ($p = 0.003$), and 2.6% ($p = 0.007$) for untreated, IL-2 MNs, IL-2+CCL22 MNs and baricitinib MNs respectively). However, T_{regs} were exclusively enriched in the AA-like lesions treated with IL-2+CCL22 MNs (**Figure 3**a,b). Together, these findings support our in vitro data suggesting that JAK inhibition is detrimental for the T_{regs}, bolstering the therapeutic merit of our combined IL-2 and CCL22 therapy which is superior to IL-2 alone. Finally, these data were supported by the histological analysis of the affected lesions confirming that mice treated with MNs had an absence of infiltrating lymphocytes including $CD3^+$ and $CD8^+$ cells (Figures 3c and S5, Supporting Information).

2.6. MN-Mediated Immunomodulation Promotes Sustained Hair Regrowth in a Model of Immune-Mediated Alopecia and Is Superior to Subcutaneous Injection

Next, we compared the effect on hair growth when delivering our immunomodulators (CCL22+IL2) or baricitinib via our MN patch, versus conventional subcutaneous injection (SubQ) with a hypodermic needle. The same treatment regimen as before was performed and mice were treated with MN patches loaded with both CCL22 (100 ng patch^{-1}) and IL-2 (10 ng patch^{-1}), baricitinib (1 ug patch^{-1}) or were administered empty MNs (**Figure 4**a). For the SubQ group, we used therapeutically equivalent dosages of IL-2+CCL22. Mice were monitored weekly, and a scoring system was used to gauge hair regrowth, as described by others.[28–30] Briefly, a score of 1 corresponds to uneven growth, poor hair density, and evident skin, whereas a score of 4 corresponds to complete restoration of highly dense hair growth. We confirmed that mice administered with IL-2+CCL22-loaded MNs displayed significant hair regrowth as early as 3 weeks post-treatment initiation compared to the untreated group (Figure 4b,c). Similarly, mice administered baricitinib MNs also displayed hair growth although the onset of action was slower compared to those administered CCL22+IL-2 MNs. Interestingly, administration of empty MNs resulted in moderate improvement in the first weeks of the treatment but plateaued at week 5 as hair regrowth was not fully prepared. Finally, no therapeutic benefit was induced by SubQ IL-2+CCL22 as evident by the lack of hair growth (Figure 4b,c). Analysis of the long-term efficacy at week 8 post-treatment initiation confirmed was no difference between empty MNs versus untreated (p-value = 0.1), but there were differences between empty versus IL-2+CCL22-loaded MNs (p-value = 0.001) and IL-2+CCL22-loaded MNs versus untreated (p-value < 0.0001). Similarly, there was no statistically significant difference between IL-2+CCL22-loaded MNs and baricitinib MNs (p-value = 0.9988). However, baricitinib MNs were superior to empty MNs (p-value < 0.0001).

2.7. ISF Sampling Using MNs Informs on T_{reg} Homing into Immune-Mediated Alopecia Lesions Following MN Treatment

To further understand the immune remodeling in the HF following treatment, we leveraged the ability of our MN platform to retrieve cellular biomarkers from ISF, which we and others have demonstrated can inform on the physiological state in the context of allo-immunity, cancer immunotherapy, and vaccination.[22,23,31] Upon removal of the patch, the hydrogel matrix of the MNs can be digested on-demand by incubating them with a reducing agent (*tris* (2-carboxyethil) phosphine; TCEP), which prompts the cleavage of the disulfide bonds present in the HA matrix and, ultimately leading to its dissolution (**Figure 5**a). After dissolving the MNs, the entrapped cells were isolated and

Figure 2. MN-mediated delivery of CCL22 and IL-2 promotes specific expansion of T_{regs} in AA lesions and restores immune privilege. a,b) Representative dot plot (left) and quantification by flow cytometry of immune infiltrates (gated as CD45+ cells) and T_{regs} (gated as $CD25^+Foxp3^+$ cells) in AA-like skin harvested at week 3 post-treatment initiation. Multiple comparisons among groups were determined using one-way ANOVA. p-value: ns = not significant, $^*p < 0.05$, $^{**}p < 0.01$, $^{***}p < 0.001$. c) Heat map showing the top 50 genes expressed differentially between the experimental groups. d) PCA plot showing distinctive clustering of the different experimental groups. e) Gene set enrichment analysis showing negative enrichment of IL6-JAK-STAT3 signaling, inflammatory response, interferon-gamma response, and antigen processing and presentation in the lesions treated with loaded MNs.

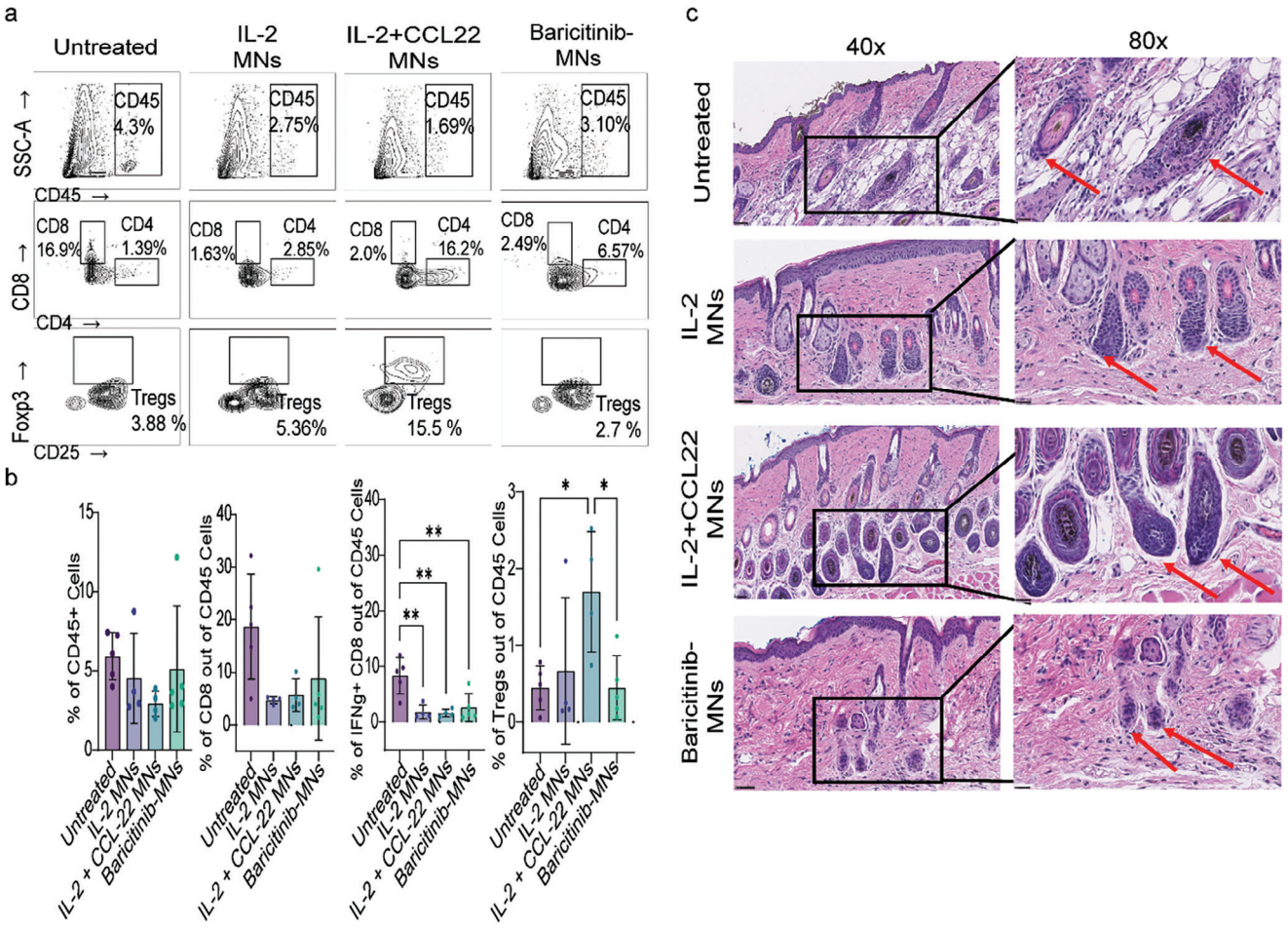

Figure 3. IL-2+CCL22 MNs induce more immune regulation than IL-2 only MNs and Baricitinib-MNs. a,b) Representative flow cytometry plots and graph of immune infiltrates (gated as $CD45^+$ cells), CD8 cells (gated as $CD45^+CD8^+$), $IFNg^+CD8$ cells (gated as $CD45^+CD8^+IFNg^+$), and T_{regs} (gated as $CD4^+CD25^+Foxp3^+$ cells) in AA-like skin harvested at week 3 post-treatment initiation. Multiple comparisons among groups were determined using one-way ANOVA. *p*-value: ns = not significant, $*p < 0.05$, $**p < 0.01$, $***p < 0.001$. c) Histological analysis of the HF structures (red arrows) by H&E staining. HF-infiltrating lymphocytes were significantly lower in IL-2 MNs and Baricitinib MNs compared to untreated, and almost no lymphocytes were infiltrating IL-2+CCL22 MNs treated HF.

analyzed by flow cytometry to enumerate the immune cells present in the lesions. Briefly, the same MNs used to deliver the immunomodulators were removed on days 1, 5, 9, and 11 post-treatment initiation and were incubated in a 10 mM solution of TCEP to dissolve them and recover the immune cells in less than 5 min. Next, T_{reg} frequencies and counts were analyzed by flow cytometry which we hypothesized would increase following the delivery of CCL22 and IL-2 as we previously confirmed in agreement with the findings in the skin. Analysis of ISF-retrieved cells from early timepoints (days 1 and 5 post-treatment initiation) revealed no significant differences between T_{reg} frequencies in mice administered with loaded MNs and those treated with empty MNs. However, T_{reg} homing into AA-like lesions treated with IL2+CCL22-loaded MNs increased significantly over time, reaching more than fivefold increase by days 9 and 11 (Figure 5b,c).

2.8. IL-2+CCL22 Delivery Using MNs Promotes Local T_{regs} Expansion in a Humanized Skin Transplant Model

Building on the findings in the AA-like model, we finally were interested in studying the therapeutic potential of our MN in a more clinically relevant setting. We first performed a penetration assay on skin from healthy donor patients undergoing cosmetic surgery, confirming that the MNs could effectively disrupt the stratum corneum as evidenced by the presence of micro-conduits that could be easily observed pre- and post-staining (**Figure 6a**). Next, we generated a humanized model by grafting healthy human skin onto the dorsal trunks of non-obese diabetic—severe combined immunodeficient (scid) IL-2 receptor-γnull (NSG) mice, as described by us before (Figure 6b).[32] We delivered 4 × 10^6 human peripheral blood mononuclear cells (PBMCs) and 1 × 10^6 T_{regs} to the mice 7 days post-transplantation (Figure 6b).

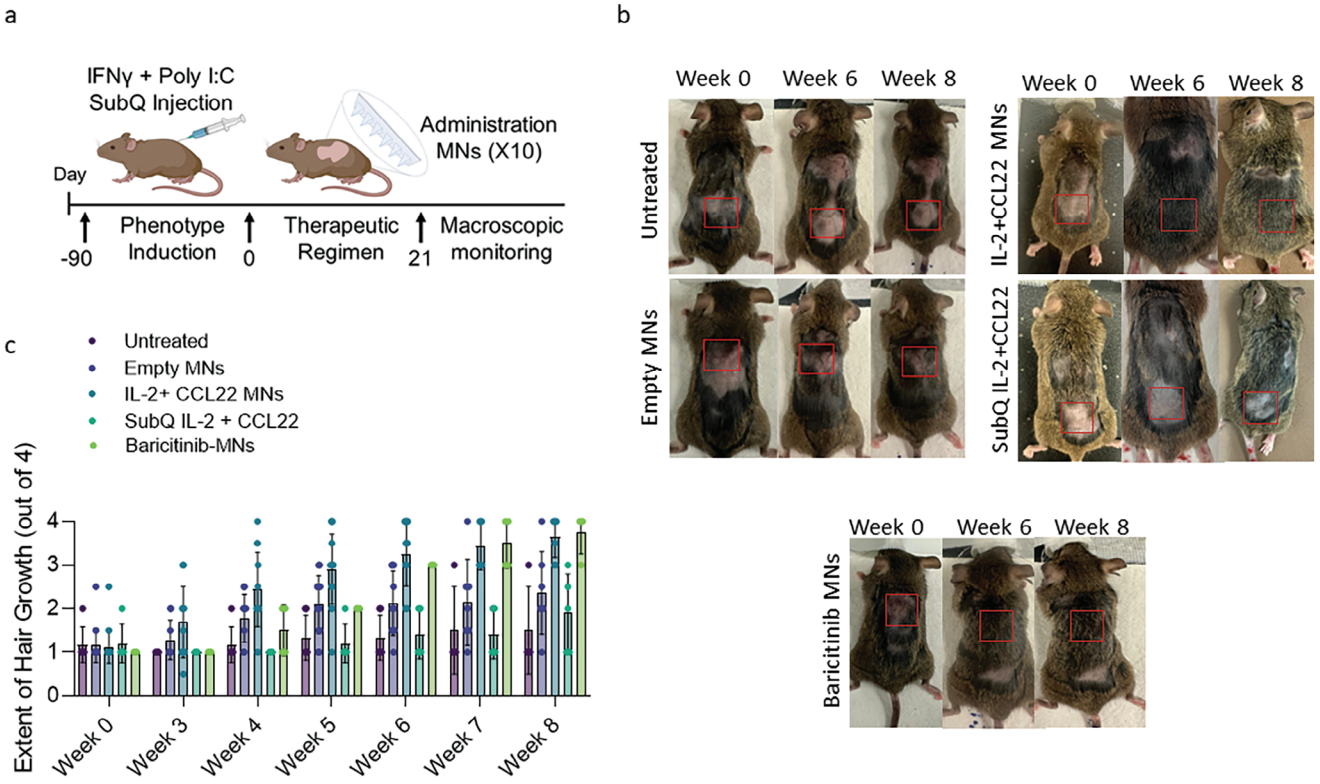

Figure 4. Delivery of immunomodulators with MNs promotes hair regrowth in an immune-mediated alopecia areata model, and is superior to subcutaneous injections. a) Schematic timeline of therapeutic regimen. C3H/HeJ mice displaying an AA-like phenotype received the following therapeutic regimen: serial application of 10 MNs patches (1 patch per lesion) for 24 h of either empty MNs, CCL22 (100 ng)+IL-2 (10 ng)-loaded MNs, or baricitinib (1 µg)-loaded MNs. b) Macroscopic assessment of hair regrowth following MN-based treatment. c) Hair regrowth scores following treatment. Mice were monitored weekly, and each lesion was blindly scored from 1 to 4 based on hair regrowth status (1 = uneven hair growth; 2 = low hair density; 3 = moderate hair density; 4 = high hair density). Statistical significance was determined using two-way Anova.

The mice were then administered serially with MNs loaded with recombinant human CCL22 (100 ng) and IL-2 (10 ng) every other day (7 patches in total) or left untreated. Following treatment, mice were sacrificed at day 21 post-transplantation for mechanistic analysis, where the immune cell populations in the human skin allografts and the spleen were enumerated by flow cytometry. Mice treated with IL2+CCL22-loaded MNs showed a significantly higher percentage of T_{regs} in the skin allografts compared to the untreated ones, demonstrating that the MNs were capable of mediating T_{reg} expansion locally. Higher percentage of T_{regs} was confirmed when gating T_{regs} within $CD45^+$ and $CD4^+$ cells as well as by mean fluorescence intensity (MFI) (Figure 6d–f). Also, we confirmed an increase in the ratio of T_{regs} to Effector ($CD45RO^+$ cells) CD8 and CD4 cells (Figure 6g,h). On the day of mechanistic analysis, we also sampled the ISF from the allograft using the MNs as described before and compared the immune signature between treated and untreated mice by flow cytometry. A significant increase in the percentage of T_{regs} was reported in the ISF sampled from MN-treated mice compared to the control group in accordance with the findings from the skin allograft analysis, supporting the potential of the MNs for minimally invasive immunosurveillance (Figure 6i).

3. Discussion

AA is an autoimmune disease driven by the disruption of immune regulation in the HFs, mainly orchestrated by autoreactive cytotoxic $CD8^+$ and $CD4^+$ effector cells that promote AA development and persistence. It has been shown that transferring $CD8^+$ cells isolated from AA-affected mice into healthy mice induces patchy AA and similarly, that transferring $CD4^+CD25^-$ cells promotes systemic AA.[33] Instead, the AA phenotype induced by both $CD8^+$ and $CD4^+CD25^-$ cells could be abolished when co-transferred with regulatory CD4 cells,[33] supporting the immune-protective role of T_{regs} in AA and their key contribution to maintaining self-tolerance.[26,33,34] Along with the constitutive expression of the transcription factor Foxp3, which regulates their suppressive function, T_{regs} also express the high-affinity IL-2 receptor alpha CD25[35–37] at higher levels than any other immune cell.[38–41] IL-2 is indispensable for T_{reg} survival, stability, and proliferation.[37,42] yet they cannot self-produce it and rely on exogenous sources.[43–45] It has been shown in different autoimmunity and alloimmunity studies that systemic delivery of low-dose IL-2 promotes peripheral T_{regs} expansion but cannot effectively reach the local areas of antigen encounter.[38,41] Moreover, even when given at low-dose, systemic IL-2 stimulates

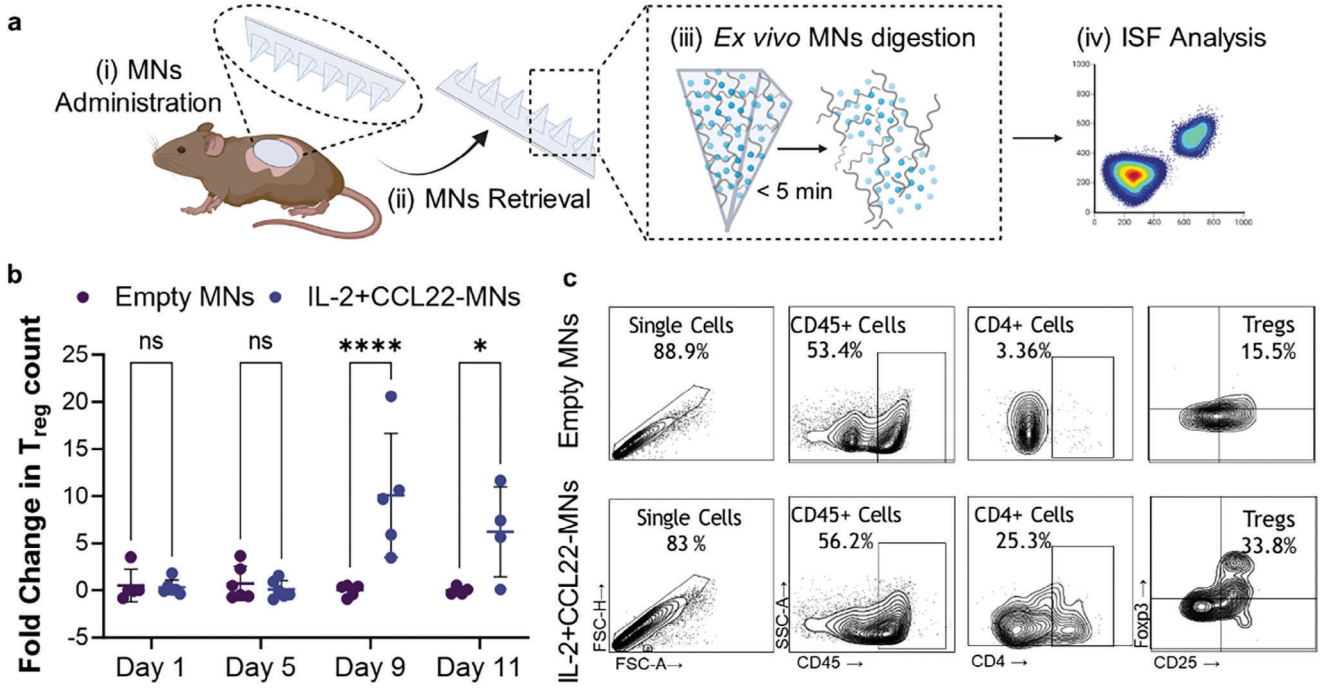

Figure 5. MNs can sample ISF from the AA-like lesions to longitudinally monitor the T_{reg} homing process. a) Schematic representation of the diagnostic compartment of the MN patch; following patch retrieval, the hydrogel matrix can be digested on-demand for facile recovery of cellular biomarkers and successive analysis. The same MNs used for treatment were recovered 24 h post-administration and digested with a 10 mM solution of TCEP to dissolve the HA matrix and recover the immune infiltrates for analysis by flow cytometry. b,c) Representative dot plot and quantification of the fold change in T_{reg} counts over time. Data are represented as mean ± s.e.m. Statistical significance was determined by one-way ANOVA. $^{**}P \leq 0.01$, $^{*}P \leq 0.05$, ns = non-significant.

concomitantly cytotoxic T cells inducing pro-inflammatory activity.[38,41]

Using single-cell transcriptomic data from public repositories, we confirmed that T_{regs} infiltrating the AA lesions (in both humans and mice) have significant upregulation of the IL-2/STAT5 signaling pathway. Since IL-2/STAT5 signaling is essential for T_{reg} homeostasis,[14,37,46,47] we hypothesized that boosting this pathway via local delivery of IL-2 could promote specific amplification of skin-resident T_{regs}, which could abolish and reverse immune-mediated alopecia and improve hair regrowth. Given its direct and exclusive application to the affected areas, our MN-based therapy would overcome the limitations of systemic delivery of IL-2 by favoring local T_{reg} proliferation at the sites of antigen encounter and prevent peripheral T_{reg} expansion. In a recent study by Cohen et al., skin-specific T_{regs} were shown to have a distinct role in preventing HF inflammation and alopecia.[12] Notably, their immune regulatory function was found to be primarily mediated by the expression of the high-affinity IL-2 receptor. Hence, localized delivery of IL-2 presents greater promise over systemic administration, as it can precisely target these skin-specific T_{regs}.

Additionally, we studied the effect of co-delivery of CCL22, a potent T_{reg} chemoattractant that we and others have demonstrated to promote migration of T_{regs} together with IL2. We proved that a combination therapy of IL-2 and CCL22, delivered locally into immune-mediated AA-like alopecia lesions using an MN patch, ensures T_{reg} recruitment to the affected skin while promoting T_{reg} proliferation, stability, and survival. Our overarching hypothesis is that chronic AA remission can only be achieved by an immunomodulatory treatment capable of suppressing the effector T cell compartment without compromising the regulatory arm of the immune system. Our in vitro data confirm that JAK inhibitors are not T_{reg}-tropic since they inhibit STAT5 signaling,[13,14] which could explain the AA relapse seen in patients after JAK inhibitor withdrawal.[15,16] This is further supported by our in vivo data, demonstrating that local JAK inhibition with Baricitinib-MNs does not enhance the number of T_{regs} that are important to generating immune tolerance. Furthermore, we demonstrated that the combination of IL-2 and CCL22 is superior to IL-2 alone, as it led to higher levels of lesional T_{regs}. Hence, we believe that our T_{reg}-centric therapy using MN-mediated delivery of IL2+CCL22 could promote long-term tolerance and reversal of the symptoms.

The design of our patch was carefully curated to enable clinical translation using a crosslinked HA matrix that is amenable for repetitive administration and offers high-loading capacity and thermal stability of embedded proteins. Here, we confirm that our MNs allow encapsulation of clinically-relevant doses of immunomodulators without impacting their mechanical properties. Others have demonstrated that dissolvable MNs can also deliver high amounts of drugs, yet in the context of AA and its remittent/relapsing course, dissolvable MNs that may need to be applied repeatedly are not desirable due to the deposition of needle-tip materials and the safety concerns associated with foreign body response. Instead, the crosslinked matrix of our proposed MN platform can effectively penetrate the stratum corneum barrier

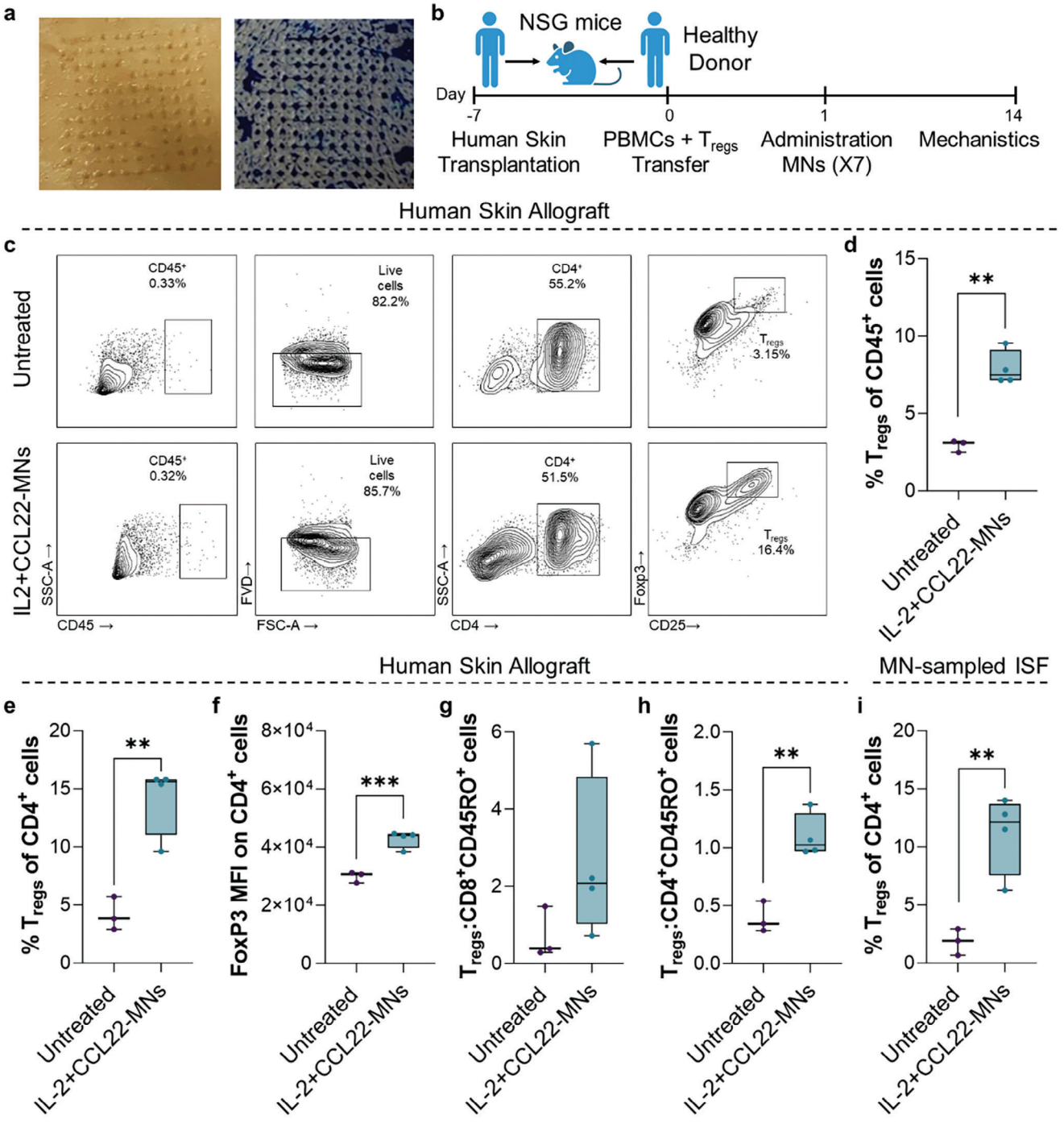

Figure 6. IL-2+CCL22-loaded MNs can recruit T_{regs} and promote their proliferation in the allografts of humanized skin transplant murine models. a) Optical microscopy demonstrating successful ex vivo penetration of a human skin explants (microconduits were left unstained (left image) or stained with Shandon Tissue-Marking Dye to facilitate visualization (right). b) Schematic representation of the humanized mouse model of skin transplantation and the experimental timeline. NSG mice were transplanted with skin grafts from healthy donors 7 days before the adoptive transfer of PBMCs enriched with T_{regs}. 24 h post-adoptive transfer, mice were administered serially with IL-2+CCL22-loaded MNs (7 applications) and euthanized at day 14 post-cell transfer and treatment initiation for mechanistic analysis ($n = 3$ for untreated and $n = 4$ for IL-2+CCL-22 Loaded MN group). c) Representative flow cytometry dot plots and quantification of T_{regs} gated as $CD4^+CD25^+Foxp3^+$, d) as% of CD45+ cells e) and as% of $CD4^+$ cells, or f) displayed by their mean fluorescence intensity (MFI) in the human skin allografts. g,h), Quantification of the ratio of T_{regs} to Effector CD4 and CD8 cells (gated as $CD4^+CD45RO+$ and CD8+CD45RO+) in the human skin allograft. i) ISF analysis using flow cytometry, MNs were digested and analyzed using flow cytometry as described before. Pairwise comparisons were performed using Student *t*-tests. $^{**}P \leq 0.01$, $^{*}P \leq 0.05$, ns = non-significant.

and upon insertion rapidly swell, forming micro-conduits to release drugs transdermally in a targeted way to the site of the immune insult, the HF, without residue deposition.

Another consideration for clinical translation is the cold chain requirements of biologics, from production to end use, to prevent aggregation, cargo denaturation, and oxidative degradation that otherwise may render them ineffective.[48] Our crosslinked HA hydrogel appears to shield the entrapped immunomodulators and prevents protein conformational changes, conferring long-term maintenance of its biological activity. We demonstrated that the biological activity of IL-2 is maintained for over 1 year when loaded into the MNs (manufacturer's guidelines confirm that protein activity once reconstituted is lost after a week if stored at room temperature). We hypothesized that multiple elements of our platform may be at play to enable the preservation of biological activity including the stabilizing effect that polyanions such as sodium hyaluronate have on cytokines via electrostatic complexation and the removal of water from the MN formulation.[49–51] Moreover, protein immobilization within the hydrogel mesh may prevent protein aggregation and ensure bioactivity upon elution from the MN patch, supporting that cold-chain requirements could be eliminated when using the patch. We further demonstrate the translational potential of our platform by virtue of its drug-agnostic properties, which allowed us to encapsulate and deliver multiple functional drugs including proteins and small molecules such as baricitinib.

Microneedling, a procedural therapy by which micro punctures are repetitively induced with derma-rollers or microneedles, has been demonstrated to promote hair regrowth in small-sized human clinical trials for patients suffering androgenetic alopecia, showing on-par efficacy to the standard-of-care treatments such as topical minoxidil or improving the outcome of those who had been therapy-resistant.[52] In the context of AA, data are scarce, and transient benefit has been only observed in specific cases when microneedling was combined with topical corticosteroids.[53,54] Yet, sustained hair regrowth in AA patients has never been reported with local approaches as none of the therapies used in combination with microneedling targeted the molecular mechanisms driving the disease. Here, our studies in an AA-like murine model displaying classic patchy areas with hair loss demonstrated that delivering the combination of T_{reg} amplifying therapeutics via our MN platform promotes superior hair regrowth than microneedling alone, or delivery of the same agents with hypodermic needles. Indeed, it has been hypothesized that the microtrauma caused by the MNs can alter the HF microenvironment as it stimulates the release of growth factors, such as platelet-derived growth factors and vascular endothelial growth factors among others.[55,56] These growth factors enhance blood flow to the HF which is vital for hair growth.[56] Furthermore, the MNs enable homogenous drug delivery into the dermal milieu, supporting our findings that delivery of immunomodulators mediated by the MNs is more effective than using a hypodermic needle in promoting hair growth. Also, our data show that only the recruitment and proliferation of T_{regs} can restore the immune equilibrium and provide a long-term benefit.

Mechanistic studies confirmed that CCL22 and IL-2 delivery resulted in skin restoration of T_{regs} and was accompanied by a reduction of the autoreactive T cell infiltrates RNA-seq of AA-like skin lesions confirmed attenuation of hallmark AA inflammatory pathways, and a significant decrease in the signature of IFNγ and IL6-JAK-STAT3 was noted in the lesions treated with IL-2+CCL-22 MNs. Similarly, the ALADIN gene signature defining AA, was downregulated in these lesions. We also used a humanized skin transplant model to interrogate the therapeutic potential of our platform, confirming that our MNs can effectively disrupt the human stratum corneum and release the drugs for local remodeling of the skin immune signature, resulting in increased frequencies of T_{regs} ultimately supporting the translation of our platform into clinical settings.

Finally, we and others have demonstrated the diagnostic value of ISF to interrogate the immune signature in the skin which correlates with the physiological state of the patient.[22,23,31,57] In the context of skin autoimmune diseases, MNs have been recently proposed to sample miRNA for psoriasis diagnosis, with more applications expected to arise to enable multiplex biomarker analysis.[58] Here, we focused on the ISF cellular compartment, demonstrating that analysis of the T_{reg} homing process into the skin lesions enables longitudinal monitoring of the dynamics of T_{reg} migration and proliferation which may ultimately offer precision therapy.

In this work, we demonstrate the therapeutic merit of immunoregulation, rather than immunosuppression, in reversing immune-mediated alopecia using MNs capable of delivering therapeutics in a targeted and non-invasive manner into the affected lesions. Using immune-mediated alopecia as a model of skin autoimmunity, we foresee that amplifying T_{regs} using our MN platform will be translated into other skin conditions with the same origin, while providing patients with non-invasive treatment and diagnosis.

4. Experimental Section

Materials: All reagents and solvents were purchased from Sigma Aldrich unless stated otherwise. Sodium hyaluronate (60 kDa) was obtained from LifeCore Medical with a purity of at least 95%. *N*-hydroxysuccinimide (NHS)-terminated 8-arm PEG (40 and 10 kDa) was purchased from Creative PEG Works. Microneedle molds were obtained from Blueacre Technology (11 × 11 needles with a height of 600 µm, base width of 300 µm, and tip to tip spacing of 600 µm). Recombinant murine CCL22, recombinant human IL-2, and recombinant murine IFN*γ* were acquired from PeproTech. poly[I:C] was purchased from InvivoGen.

Synthesis of Amino-Modified Hyaluronic Acid (HA-SS-NH_2) Polymer: The HA-SS-NH_2 polymer was synthesized as previously described. Briefly, 60 kDa-sodium hyaluronate (1% w/v in MES buffer) was activated with *N*-(3-(dimethylamino)propyl)carbodiimide and NHS at a 1:4:2 molar ratio and reacted at room temperature for 30 min under magnetic stirring. Next, the activated hyaluronic acid (HA) was mixed under vigorous stirring with cysteamine dihydrochloride (1:10 molar ratio) and allowed to react at room temperature for 12 h. The resulting HA-SS-NH_2 polymer was purified by dialysis against deionized water for 5 days, freeze-dried, and stored at −20 °C protected from humidity until use. Structural analysis of the polymer was performed by ^{1}H-NMR using D_2O as a solvent (400 MHz Varian NMR spectrometer).

Fabrication HA-Based MNs: MNs were synthesized as described by the authors.[22] Briefly, an initial layer of HA-SS-NH_2 (10% w/v in phosphate buffer, pH = 7.4) was deposited on top of the MN molds and these were centrifuged at 4200 rpm for 5 min followed by a freeze-drying step. Next, a second layer of 8-arm-PEG-NHS crosslinker (70:30 volume ratio of 40 kDa: 10 kDa crosslinker, 10% w/v in phosphate buffer, pH = 7.4) was deposited on the mold, centrifuged again at 4200 rpm for 5 min followed and freeze-dried. An aqueous solution containing glycine (10 ng mL^{-1})

and the therapeutic agents CCL22 (10 ng mL^{-1}) and IL-2 (10 ng mL^{-1}) or baricitnib (1 µg mL^{-1}) was then deposited drop-wise on top of the molds and briefly spun for 1 min to concentrate the drug in the needle-like projections. Finally, a layer of PLGA (Resomer RG 858 S, Sigma Aldrich, USA) at 15% (w/v) serving as the backing layer of the patch was deposited on top of the molds dropwise until covering the whole area (200 µL). MNs were allowed to dry at room temperature for 12 h, peeled off the molds, and stored until use. Empty MNs were fabricated in a similar manner; following the addition of the crosslinking layer, the backing layer was deposited immediately after and allowed to dry as described.

Assessment of the Structure and Mechanical Strength of the HA-Based MNs: MNs were imaged by scanning electron microscopy (SEM) using a JSM-6610 LV SEM microscope. Mechanical strength as a function of drug loading was determined using a micro-force test station with a mechanical sensor (3400 Series, Instron, USA). Briefly, MNs loaded with increasing amounts of CCL22 and IL-2 were mounted on the surface of the platform with the projections facing up, and increasing forces were applied. The displacement and forces were recorded from the moment the sensors touched the uppermost tip of the MNs until a maximum force of ≈100 N was reached. Force–travel curves of MNs arrays were obtained by correlating the compressive strain or displacement (%) with the compressive stress (kPa). Young's modulus was calculated from the slope in the elastic (or linear) portion of the physical stress–strain curve (GPa).

Mass Spectrum Analysis of Protein Structure: The structure of released proteins from the MNs was compared to the native ones by mass spectrometry. Briefly, IL-2-loaded MNs were incubated in PBS for 24 h under physiological conditions (37 °C, pH = 7.4) and the supernatants were recovered. The spectra of released and native IL-2 were detected using a 6100 Series Single Quadrupole LC/MS with a ZORBAX 300StableBond column.

In Vitro Characterization of Cytokine Activity as a Function of Storage Temperature and Time: MNs loaded with 10 ng of IL-2 were fabricated and stored at different temperatures (room temperature, 4 and −20 °C) and for increasing durations (1 week, 1, 4, 10 months, and 1 year old). To assess cytokine activity, MNs were incubated with 75 K T_{regs} at 37 °C in a 96-well plate. T_{reg} stability and survival were assessed using flow cytometry. The following antibodies were used: CD4 V500 (Biolegend 560782), CD25 PE (Biolegend 101904), Foxp3 APC (eBioscience17-5773-82), Fixed Viability Dye (FVD) eFluor780 (eBioscience).

Induction of AA-Like Phenotype in C3H/HeJ Mice: C3H/HeJ mice were purchased from The Jackson Laboratory (Bar Harbour, ME, USA) and housed under specific-pathogen-free conditions at the Brigham and Women's Hospital animal facility. All animal work was performed in compliance with ethical regulations and was approved by the Institutional Animal Care and Use Committee of Brigham and Women's Hospital. AA-like phenotype in mice was induced as described by Shin and colleagues.[25] Briefly, 15-week-old female mice were injected subcutaneously with a mixture of IFNγ (2×10^4 units mice^{-1}) and poly (I:C) (100 µg mice^{-1}). Mice were injected in two spots in the dorsal area twice per week for 8 weeks and the development of patchy AA lesions was monitored until treatment completion.

Animal Studies: 4 weeks post phenotype induction, all lesions were delineated to consistently apply the MNs in the same spot throughout the experiment. Briefly, mice were left untreated (control group) or administered ten times every other day with either empty MNs, MNs loaded with CCL22 and IL-2 (100 ng and 10 ng respectively), MNs loaded with IL-2 (10 ng) or MNs loaded with baricitnib (1 µg). Briefly, MNs were administered on top of the lesions by thumb-pressing the patch for 30 s and secured with medical-grade tape (FlexCon, USA) for 24 h. Hair growth following treatment was evaluated weekly using a scoring system proposed by others where each lesion was ranked based on its hair density and degree of visible skin.[28–30] Additionally, mechanistic analysis studies were performed at week 3 ($n = 6$ or 7 mice per experimental group) and week 6 post-treatment initiation ($n = 4$ or 5 per experimental group).

Analysis of T_{reg} and Effector T Cell Distribution by Immunohistochemistry: Skin tissue sections from AA lesions were processed by the Hope Babette Tang Histology facility at the Koch Institute of Integrative Cancer Research at MIT (Cambridge, USA) and analyzed using the Aperio ImageScope 12.3.3 software (Leica). Briefly, 0.5 cm^2 skin sections harvested on the day of mechanistic analysis were embedded in OCT, flash-frozen, and preserved at −80 °C until sectioning. Skins were cryosectioned into 5 µm-wide tissue sections and FOXP3, CD8, and CD3 expression was confirmed via indirect staining using HRP-conjugated antibodies and visualized using DAB substrate. Last, slides were counterstained with Hematoxylin (coloring nuclei in blue).

Analysis of AA Skin Lesions and Lymphoid Tissues by Flow Cytometry: On the day of mechanistic analysis, skin lesions, draining lymph nodes, and spleens were harvested and processed accordingly. Immune infiltrates from the skin lesions were isolated as follows: 0.5 cm^2 skin sections were thoroughly minced and processed as described by Sakamoto and colleagues.[59] Spleens and LNs were mechanically dissociated, filtered through a 40 µm nylon cell strainer, and spleen suspensions were further treated with ACK lysing buffer (Gibco) for 1 min. Isolated cells from all tissues were reconstituted at a maximum concentration of 1×10^6 cells in 100 µL FACS staining buffer (1× DPBS, 1% Bovine Serum Albumin, 0.02% sodium azide (Sigma Aldrich)) for flow cytometry analysis. For cytokines analysis, Skin cells were stimulated with PMA (100 ng mL^{-1}, MilliporeSigma), ionomycin (1 ug mL^{-1}, MilliporeSigma), and Brefeldin A (10 ug mL^{-1}, MilliporeSigma) at 37 °C for 4 h prior to flow cytometry staining. The following anti-mouse antibodies were purchased from eBioscience: CD45 PE-Cy7(clone 30-F11), FOXP3 APC (clone FJK-16S), CD4 PE (clone RM4-5), and BD Biosciences: CD8 BUV805 (Cat# 612898), TNFa BV785 (Cat# 506341), IFNg FITC (Cat# 505806) CD44 BV711 (Cat# 103057). Dead cells were stained using FVD eFluor780 (eBioscience). Stained cells were analyzed by flow cytometry using a BD FACS Canto II cytometer (BD Biosciences) and all data were analyzed using FlowJo version 10 (Flowjo LLC).

Analysis of MN-Sampled ISF from AA Lesions: ISF was sampled from AA lesions using MNs as described by the authors. Following retrieval from mice, MNs were immersed in a solution of 10 mM TCEP in PBS (pH = 7.4) and incubated at 37 °C for 10 min to allow digestion of the polymeric matrix. Next, samples were centrifuged at 1200 rpm to pellet the cells and the recovered cellular suspension was filtered with a 70 µm cell strainer (BD bioscience) prior to staining and analysis by flow cytometry.

Gene Expression Analysis in AA Lesions by Quantitative Real-Time Polymerase Chain Reaction (qPCR): On the day of mechanistic analysis, a 0.5 cm^2 piece of skin was excised from the AA lesion and kept in RNAprotect tissue reagent (Qiagen, Cat. #76104) at −80 °C until processing. Briefly, skin sections were partially thawed and cut into 0.5 mm^2 pieces for RNA isolation (Qiagen RNeasy plus Mini Kit, Cat.# 4136) following the manufacturer's protocol. The concentration of eluted RNA was measured with a NanoDrop 2000 Spectrophotometer (Thermofisher Scientific, Waltham, MA, United States) and the complementary DNA strands were reverse transcribed with iScript Reverse Transcription Supermix (#1708841, Bio-Rad Laboratories) as per the manufacturer's protocol and preserved at −20 °C till further use. Quantitative real-time PCR was performed in 0.1 mL MicroAmp Fast Optical 96-Well Reaction Plates (Applied Biosystems, #4346906) with 30 ng of ds-RNA per mRNA target, 500 nm forward and 500 nm reverse primers, and SsoAdvanced Universal SYBR Green Supermix (#1725274, Bio-Rad Laboratories) diluted to 1× with PCR-grade water (#W4502, Sigma Aldrich) in 10-µL reaction volumes. Primer pairs were based on OriGene's qSTAR qPCR Primer Pairs (Rockville, MD, United States) and synthesized through Integrated DNA Technologies (Coralville, IA, United States). Cycle threshold (Ct) values were measured with QuantStudio 3 (Thermofisher Scientific, Waltham, MA, United States). Ct values were then corrected with GAPDH housekeeping gene expression per replicate, per run, log2 normalized, averaged for the control replicates, and deviation from the average was calculated per condition, per replicate. Fold change of FOXP3 to GAPDH was calculated by dividing fold change of FOXP3 to fold change of GAPDH and fold change of IFNɣ was presented after normalization to GAPDH.

Gene Expression Analysis by Bulk RNA Sequencing: Quality checks of the raw reads in FASTQ format were performed using FastQC and MultiQC (FastQC citation: Andrews S. 2010. FastQC A Quality Control Tool for High Throughput Sequence Data. https://www.bioinformatics.babraham.ac.uk/projects/fastqc/, MultiQC.[60]). Then, The reads were aligned to the mouse reference genome (mm39) using HISAT2 v2.2.1.[61] The aligned

reads in SAM format were then sorted and a BAM file for each sample was generated using SAMtools v1.12.[62] Post alignments checks were performed using Deeptools version 3.5.1[63] and RSeQC version 5.0.1.[64] Counting raw reads over the genomic features was performed using featureCounts version 1.6.5[65] in the presence of an annotation reference in GTF format obtained from GENCODE vM29 with parameters -t gene -g gene_name -s 2 -p -B. Genes with raw read counts sum less than 10 across all the samples were excluded. DESeq2 version 1.34.0 was used to perform the differential expression analysis.[66] Genes with an absolute log2 fold change greater than 1 and *p*-adjusted value less than 0.05 were considered differentially expressed. Gene set enrichment analysis for both the up- and down-regulated genes was done using GSEA v4.3.2 from Broad Institute.[67,68]

Analysis of Publicly Available Single-Cell RNA-Seq Data: AA and control human and mouse single-cell RNA-seq data (PRJNA606026) were analyzed separately for each species. "NormalizeData," "FindVariableFeatures," and "ScaleData" functions were applied for each sample from the Seurat R package version 4.0.5.[69] Then, the integration and batch effect correction step was performed using the "FindIntegrationAnchors" followed by "IntegrateData" functions. After that, "RunPCA" and "RunUMAP" were applied to reduce the dimensionality of the data by setting the "dims" parameter to 35, and cells were clustered with resolution 0.5.

Statistical Analysis: Statistical analyses were carried out using GraphPad Prism 8 (GraphPad Software). A minimum of $n = 4$ biological replicates were used per condition in in vitro experiments. Pairwise comparisons were performed using Student *t*-tests. Multiple comparisons among groups were determined using one-way ANOVA followed by a post-hoc test. For in vivo experiments, a minimum of $n = 4$ biological replicates were used per condition in each experiment. AA mice were randomly assigned to the different experiment groups, and a blinded investigator performed hair growth scoring. Multiple comparisons among groups were determined using one-way ANOVA. Two-way ANOVA was used to compare hair growth at the different time points. No specific pre-processing of data was performed prior to statistical analyses. Data were analyzed by Grubbs' test for statistical outliers, which were pre-defined using an alpha value of 0.01. Differences between groups were considered significant at *p*-values below 0.05 ($*p < 0.05$, $**p < 0.01$, $***p < 0.001$).

Supporting Information

Supporting Information is available from the Wiley Online Library or from the author.

Acknowledgements

The authors thank the Department of Medicine at Brigham and Women's Hospital for the Ignite Fund Award and the Shark Tank Fund Award that supported this work.

Conflict of Interest

The authors declare no conflict of interest.

Author Contributions

N.Y. and N.P. contributed equally to this work. N.Y., N.P., N.A., and J.R.A. conceived the work and designed the studies. N.Y. and N.P. performed the in vitro and in vivo experiments and analyzed the data. A.E.K. performed the in-silico studies. A.B., D.Z., and A.S. supported in vivo studies. D.C., A.D., T.H., C.D., and A.H. contributed to data collection. J.C., P.D., and C.L. provided comments. N.Y., N.P., N.A., and J.R.A. wrote and reviewed the manuscript.

Data Availability Statement

The data that support the findings of this study are available from the corresponding author upon reasonable request.

Keywords

autoimmunity, drug delivery, immunoregulation microneedles, skin disorders

Received: November 13, 2023
Revised: April 5, 2024
Published online: June 5, 2024

[1] A. W. Ho, T. S. Kupper, *Nat. Rev. Immunol.* **2019**, *19*, 490.
[2] H. Ujiie, *Exp. Dermatol.* **2019**, *28*, 642.
[3] L. A. Kalekar, M. D. Rosenblum, *Int. Immunol.* **2019**, *31*, 457.
[4] C. R. Grant, R. Liberal, G. Mieli-Vergani, D. Vergani, M. S. Longhi, *Autoimmun. Rev.* **2015**, *14*, 105.
[5] A. Gilhar, A. Etzioni, R. Paus, *N. Engl. J. Med.* **2012**, *366*, 1515.
[6] C. H. Pratt, L. E. King, A. G. Messenger, A. M. Christiano, J. P. Sundberg, *Nat. Rev. Dis. Primers* **2017**, *3*, 17011.
[7] H. H. Lee, E. Gwillim, K. R. Patel, T. Hua, S. Rastogi, E. Ibler, J. I. Silverberg, *J. Am. Acad. Dermatol.* **2020**, *82*, 675.
[8] E. Darwin, P. Hirt, R. Fertig, B. Doliner, G. Delcanto, J. Jimenez, *Int. J. Trichology* **2018**, *10*, 51.
[9] A. Mostaghimi, W. Gao, M. Ray, L. Bartolome, T. Wang, C. Carley, N. Done, E. Swallow, *JAMA Dermatol.* **2023**, *159*, 411.
[10] M. Bertolini, K. McElwee, A. Gilhar, S. Bulfone-Paus, R. Paus, *Exp. Dermatol.* **2020**, *29*, 703.
[11] F. N. Hamed, A. Åstrand, M. Bertolini, A. Rossi, A. Maleki-Dizaji, A. G. Messenger, A. J. G. McDonagh, R. Tazi-Ahnini, *PLoS One* **2019**, *14*, 0210308.
[12] J. N. Cohen, V. Gouirand, C. E. Macon, M. M. Lowe, I. C. Boothby, J. M. Moreau, I. K. Gratz, A. Stoecklinger, C. T. Weaver, A. H. Sharpe, R. R. Ricardo-Gonzalez, M. D. Rosenblum, *Sci. Immunol.* **2024**, *9*, eadh0152.
[13] W. Vainchenker, S. N. Constantinescu, *Oncogene* **2013**, *32*, 2601.
[14] M. A. Burchill, J. Yang, C. Vogtenhuber, B. R. Blazar, M. A. Farrar, *J. Immunol.* **2007**, *178*, 280.
[15] D. Yan, H. Fan, M. Chen, L. Xia, S. Wang, W. Dong, Q. Wang, S. Niu, H. Rao, L. Chen, X. Nie, Y. Fang, *Front. Pharmacol.* **2022**, *13*.
[16] Ö. Aşkın, D. Özkoca, T. K. Uzunçakmak, S. Serdaroğlu, *Dermatol. Ther.* **2021**, *34*, e14746.
[17] D. P. McLornan, J. E. Pope, J. Gotlib, C. N. Harrison, *Lancet* **2021**, *398*, 803.
[18] K. L. Winthrop, S. B. Cohen, *Nat. Rev. Rheumatol.* **2022**, *18*, 301.
[19] V. K. Kuchroo, P. S. Ohashi, R. B. Sartor, C. G. Vinuesa, *Nat. Med.* **2012**, *18*, 42.
[20] M. Friedel, I. A. P. Thompson, G. Kasting, R. Polsky, D. Cunningham, H. T. Soh, J. Heikenfeld, *Nat. Biomed. Eng.* **2023**, *7*, 1541.
[21] A. Mandal, A. V. Boopathy, L. K. W. Lam, K. D. Moynihan, M. E. Welch, N. R. Bennett, M. E. Turvey, N. Thai, J. H. Van, J. C. Love, P. T. Hammond, D. J. Irvine, *Sci. Transl. Med.* **2018**, *10*, eaar2227.
[22] N. Puigmal, P. Dosta, Z. Solhjou, K. Yatim, C. Ramírez, J. Y. Choi, J. B. Alhaddad, A. P. Cosme, J. Azzi, N. Artzi, *Adv. Funct. Mater.* **2021**, *31*, 2100128.
[23] P. Dosta, N. Puigmal, A. M. Cryer, A. L. Rodríguez, E. Scott, R. Weissleder, M. A. Miller, N. Artzi, *Theranostics* **2023**, *13*, 1.
[24] N. Borcherding, S. Crotts, L. S. Ortolan, N. Henderson, N. L. Bormann, A. Jabbari, *JCI Insight* **2020**, *5*, 137424.

[25] J.-M. Shin, D.-K. Choi, K.-C. Sohn, J.-W. Koh, Y. H. Lee, Y.-J. Seo, C. D. Kim, J.-H. Lee, Y. Lee, *Sci. Rep.* **2018**, *8*, 12518.
[26] Z. Dai, E. H. C. Wang, L. Petukhova, Y. Chang, E. Y. Lee, A. M. Christiano, *Sci. Adv.* **2021**, *7*, 1866.
[27] L. Xing, Z. Dai, A. Jabbari, J. E. Cerise, C. A. Higgins, W. Gong, A. de Jong, S. Harel, G. M. DeStefano, L. Rothman, P. Singh, L. Petukhova, J. Mackay-Wiggan, A. M. Christiano, R. Clynes, *Nat. Med.* **2014**, *20*, 1043.
[28] M. S. Orasan, I. I. Roman, A. Coneac, A. Muresan, R. I. Orasan, *Clujul Med.* **2016**, *89*, 327.
[29] G.-H. Park, K.-Y. Park, H.-I. l. Cho, S.-M. Lee, J. S. Han, C. H. Won, S. E. Chang, M. W. Lee, J. H. Choi, K. C. Moon, H. Shin, Y. J. Kang, D. H. Lee, *J. Med. Food* **2015**, *18*, 354.
[30] M. S. Orasan, P. Bolfa, A. Coneac, A. Muresan, C. Mihu, *Ann. Dermatol.* **2016**, *28*, 65.
[31] A. Mandal, A. V. Boopathy, L. K. W. Lam, K. D. Moynihan, M. E. Welch, N. R. Bennett, M. E. Turvey, N. Thai, J. H. Van, J. C. Love, P. T. Hammond, D. J. Irvine, *Sci. Transl. Med.* **2018**, *10*, eaar2227.
[32] S. K. Eskandari, I. Sulkaj, M. B. Melo, N. Li, H. Allos, J. B. Alhaddad, B. Kollar, T. J. Borges, A. S. Eskandari, M. A. Zinter, S. Cai, J. P. Assaker, J. Y. Choi, B. S. Al Dulaijan, A. Mansouri, Y. Haik, B. A. Tannous, W. J. van Son, H. G. D. Leuvenink, B. Pomahac, L. V. Riella, L. Tang, M. A. J. Seelen, D. J. Irvine, J. R. Azzi, *Sci. Transl. Med.* **2020**, *12*, eaaw4744.
[33] K. J. McElwee, P. Freyschmidt-Paul, R. Hoffmann, S. Kissling, S. Hummel, M. Vitacolonna, M. Zöller, *J. Invest. Dermatol.* **2005**, *124*, 947.
[34] E. Castela, F. Le Duff, C. Butori, M. Ticchioni, P. Hofman, P. Bahadoran, J.-P. Lacour, T. Passeron, *JAMA Dermatol.* **2014**, *150*, 748.
[35] A. Y. Rudensky, *Immunol. Rev.* **2011**, *241*, 260.
[36] P. Georgiev, L. M. Charbonnier, T. A. Chatila, *J. Clin. Immunol.* **2019**, *39*, 623.
[37] T. Chinen, A. K. Kannan, A. G. Levine, X. Fan, U. Klein, Y. Zheng, G. Gasteiger, Y. Feng, J. D. Fontenot, A. Y. Rudensky, *Nat. Immunol.* **2016**, *17*, 1322.
[38] S. Dong, K. J. Hiam-Galvez, C. T. Mowery, K. C. Herold, S. E. Gitelman, J. H. Esensten, W. Liu, A. P. Lares, A. S. Leinbach, M. Lee, V. Nguyen, S. J. Tamaki, W. Tamaki, C. M. Tamaki, M. Mehdizadeh, A. L. Putnam, M. H. Spitzer, C. J. Ye, Q. Tang, J. A. Bluestone, *JCI Insight* **2021**, *6*, 147474.
[39] C. Ye, D. Brand, S. G. Zheng, *Signal Transduction Targeted Ther.* **2018**, *3*, 2.
[40] F. Harris, Y. A. Berdugo, T. Tree, *Clin. Exp. Immunol.* **2023**, *211*, 149.
[41] T. Y. Lim, E. Perpiñán, M.-C. Londoño, R. Miquel, P. Ruiz, A. S. Kurt, E. Kodela, A. R. Cross, C. Berlin, J. Hester, F. Issa, A. Douiri, F. H. Volmer, R. Taubert, E. Williams, A. J. Demetris, A. Lesniak, G. Bensimon, J. J. Lozano, M. Martinez-Llordella, T. Tree, A. Sánchez-Fueyo, *J. Hepatol.* **2023**, *78*, 153.
[42] T. Hirai, T. L. Ramos, P. Lin, F. Simonetta, L. Su, M. Mavers, W. J. Leonard, B. Blazar, R. Negrin, et al., *J. Clin. Invest.* **2021**, *131*, 139991.
[43] B. I. Moon, T. H. Kim, J. Y. Seoh, *PLoS One* **2015**, *10*, 0141864.
[44] E. M. Shevach, *Trends Immunol.* **2012**, *33*, 626.
[45] R. Setoguchi, S. Hori, T. Takahashi, S. Sakaguchi, *J. Exp. Med.* **2005**, *201*, 723.
[46] S. A. Mahmud, L. S. Manlove, M. A. Farrar, *JAK-STAT.* **2013**, *2*, e23154.
[47] D. M. Jones, K. A. Read, K. J. Oestreich, *J. Immunol.* **2020**, *205*, 1721.
[48] R. P. Welch, H. Lee, M. A. Luzuriaga, O. R. Brohlin, J. J. Gassensmith, *Bioconjugate Chem.* **2018**, *29*, 2867.
[49] E. Sedlák, D. Fedunová, V. Veselá, D. Sedláková, M. Antalík, *Biomacromolecules* **2009**, *10*, 2533.
[50] B. Marco-Dufort, J. R. Janczy, T. Hu, M. Lütolf, F. Gatti, M. Wolf, A. Woods, S. Tetter, B. V. Sridhar, M. W. Tibbitt, *Sci. Adv.* **2022**, *8*, eabo0502.
[51] B. V. Sridhar, J. R. Janczy, Ø. Hatlevik, G. Wolfson, K. S. Anseth, M. W. Tibbitt, *Biomacromolecules* **2018**, *19*, 740.
[52] L. Bao, L. Gong, M. Guo, T. Liu, A. Shi, H. Zong, X. Xu, H. Chen, X. Gao, Y. Li, *J. Cosmet. Laser Ther.* **2020**, *22*, 1.
[53] R. Dhurat, S. Mathapati, *Indian J. Dermatol.* **2015**, *60*, 260.
[54] B. Chandrashekar, V. Yepuri, V. Mysore, *J Cutaneous Aesthetic Surg.* **2014**, *7*, 63.
[55] C. M. Giorgio, G. Babino, S. Caccavale, T. Russo, A. B. De Rosa, R. Alfano, E. Fulgione, G. Argenziano, *Clin. Exp. Dermatol.* **2020**, *45*, 323.
[56] Y. S. Kim, K. H. Jeong, J. E. Kim, Y. J. Woo, B. J. Kim, H. Kang, *Ann. Dermatol.* **2016**, *28*, 586.
[57] A. Himawan, L. K. Vora, A. D. Permana, S. Sudir, A. R. Nurdin, R. Nislawati, R. Hasyim, C. J. Scott, R. F. Donnelly, *Adv. Healthcare Mater.* **2023**, *12*, 2202066.
[58] B. H. J. Gowda, M. G. Ahmed, U. Hani, P. Kesharwani, S. Wahab, K. Paul, *Int. J. Pharm.* **2023**, *632*, 122591.
[59] K. Sakamoto, S. Goel, A. Funakoshi, T. Honda, K. Nagao, *STAR Protoc.* **2022**, *3*, 101052.
[60] P. Ewels, M. Magnusson, S. Lundin, M. Käller, *Bioinformatics* **2016**, *32*, 3047.
[61] D. Kim, B. Langmead, S. L. Salzberg, *Nat. Methods* **2015**, *12*, 357.
[62] H. Li, B. Handsaker, A. Wysoker, T. Fennell, J. Ruan, N. Homer, G. Marth, G. Abecasis, R. Durbin, *Bioinformatics* **2009**, *25*, 2078.
[63] F. Ramírez, F. Dündar, S. Diehl, B. A. Grüning, T. Manke, *Nucleic Acids Res.* **2014**, *42*, W187.
[64] L. Wang, S. Wang, W. Li, *Bioinformatics* **2012**, *28*, 2184.
[65] Y. Liao, G. K. Smyth, W. Shi, *Bioinformatics* **2014**, *30*, 923.
[66] M. I. Love, W. Huber, S. Anders, *Genome Biol.* **2014**, *15*, 550.
[67] A. Subramanian, P. Tamayo, V. K. Mootha, S. Mukherjee, B. L. Ebert, M. A. Gillette, A. Paulovich, S. L. Pomeroy, T. R. Golub, E. S. Lander, J. P. Mesirov, *Proc. Natl. Acad. Sci. U. S. A.* **2005**, *102*, 15545.
[68] V. K. Mootha, C. M. Lindgren, K.-F. Eriksson, A. Subramanian, S. Sihag, J. Lehar, P. Puigserver, E. Carlsson, M. Ridderstråle, E. Laurila, N. Houstis, M. J. Daly, N. Patterson, J. P. Mesirov, T. R. Golub, P. Tamayo, B. Spiegelman, E. S. Lander, J. N. Hirschhorn, D. Altshuler, L. C. Groop, *Nat. Genet.* **2003**, *34*, 267.
[69] R. Satija, J. A. Farrell, D. Gennert, A. F. Schier, A. Regev, *Nat. Biotechnol.* **2015**, *33*, 495.